Oxid Met (2010) 74:215–238
DOI 10.1007/s11085-010-9207-5

ORIGINAL PAPER

Influence of the Oxygen Partial Pressure on the Oxidation of Inconel 617 Alloy at High Temperature

A. Duval · F. Miserque · M. Tabarant · J.-P. Nogier · A. Gédéon

Received: 12 May 2010 / Revised: 6 August 2010 / Published online: 24 August 2010

Abstract Ni-based superalloy Inconel 617 (IN617) is one of the main candidate structural materials for high temperature components (heat exchanger) of the gas-cooled fast reactor (GFR), a possible candidate for generation IV nuclear reactor. The material in operating conditions will be exposed to impure He at a temperature of around 850 °C. The impurities are expected to be oxidizing (such as O_2, H_2O) but since no feedback experience is available for this type of reactor, the level of impurities is completely unknown. Hence, an attempt has been made to understand the influence of oxygen partial pressure on oxide composition and on the oxidation mechanisms of IN617 at 850 °C. To achieve this, oxidation tests were performed at 3 different range of partial pressure: 10^{-5}, 0.2 and 200 mbar. Tests were performed from 1 h to 28 days and the obtained oxide layers were characterized using MEB, EDX, XPS, XRD and GD-OES. The oxide layers were mainly composed of chromia containing TiO_2 and thickening with time. Aluminium oxide formed internally. Other oxides were detected in the scale, such as NiO, CoO, MoO_3 and MnO_2, except for the lowest oxygen partial pressure experiments, where a selective oxidation took place. The scale-growth mechanism was cationic for low and medium oxygen partial pressure conditions. A growth following a transient oxidation mechanism was observed for high oxygen partial pressure.

A. Duval · M. Tabarant
Laboratoire de réactivité des surfaces et interfaces, Département de physique-chimie, CEA Saclay, 91191 Gif-sur-Yvette, France

F. Miserque (✉)
Laboratoire d'étude de la corrosion aqueuse, Département de physique-chimie, CEA Saclay, 91191 Gif-sur-Yvette, France
e-mail: frederic.miserque@cea.fr

J.-P. Nogier · A. Gédéon
Laboratoire des systèmes interfaciaux à l'échelle nanométrique (UMR 7142), Université P. et M. Curie, 4 place Jussieu, 75252 Paris Cedex 5, France

Keywords Alloy 617 · High temperature oxidation · Oxide layer

Introduction

As a candidate Generation IV nuclear reactor, the gas-cooled fast reactor (GFR) is currently studied by several countries such as France, Japan, Switzerland and Euratom member countries. One of the research area concerns the choice of the various structural materials that will design the different reactor components.

Concerning the high-temperature metallic components, Ni-based alloys such as IN617, Alloy 230, Hastelloy X and Hastelloy XR, and Steels such as Incolloy 800H, 360FR, Gr22, Gr23, Gr91 and Gr92 are considered [1]. Such components include piping and heat exchangers, where the reference He-cooled design operates with an outlet temperature of 850 °C [2]. Ni-based alloys are particularly resistant to high temperature and among them, it appears that Inconel 617, which has been developed earlier for gas-cooled reactor projects, is considered as a leading candidate [1].

Several works have been done on nickel superalloys exposed to impure helium in High Temperature Gas-cooled Reactors conditions [3–11]. But in this type of reactor, impurities contained in the gas reacted with the graphite core to form carbonated impurities (such as CH_4, CO). This added to the high temperature oxidation problem some carburization/decarburization phenomenon. However, the proposed GFR reactor is expected to contain no graphite core. Hence the composition of impurities should be different with a lower level of carbonated gas and more moisture and oxygen [1] coming from leak problems or degassing.

Unlike HTGRs, no experience feedback is available on GFR, so the level of impurity is completely unknown. It will mainly depend on the He purification system that will be chosen. It is then of particular interest to understand the influence of partial pressure of an impurity gas on the oxidation.

Under oxidizing conditions, High-temperature resistant superalloys such as IN617 are able to develop a protective oxide layer. The oxide layer plays a protective role on the layer if (1) the growth of the oxide scale is parabolic, (2) the oxide formed is thermodynamically stable and has a high melting point, (3) diffusion through the oxide is slow, which will limit exchanges phenomena through the layer with its thickening and eventually stop its growth. Ni-based superalloys generally develop a protective oxide layer composed of Cr_2O_3, Al_2O_3 and/or SiO_2 oxides.

Several studies have been achieved on high temperature oxidation of IN617 [12–15]. Christ et al. [15] have studied the oxidation of IN617 at 850 °C under high and very low O_2 containing atmospheres. Under 10^{-19} bar of O_2, only Cr_2O_3, TiO and Al_2O_3 are able to form (SiO_2 is thermodynamically stable but, owing to the low Si content, will not form for kinetic reasons [11]). The oxide layer consisted of an external Cr_2O_3 layer enriched with Ti, with internal Al_2O_3. In air, the same oxide morphology is found at the steady state, after a transient period of oxidation forming a thin layer of Ni and Co oxide at the surface. Jang et al. found a duplex NiO–Cr_2O_3 layer with intergranular Al_2O_3 oxides at 900 °C when oxidizing IN617 in air for 1000 h. This oxide layer composition is expected to be found in this present study.

In spite of a same weight gain, the oxide layer grown in air appeared to be much less dense that the one grown in low oxidizing atmosphere (3.2 ppm of oxidizing gases). At 1050 °C, Jo et al. [13] found that the oxide growth rate was higher in air than in lower O_2-containing atmosphere (0.45 mbar of O_2), but evaporation of chromium oxide occurred in air environment. Indeed, at high temperature (generally above 1000 °C), CrO_3 evaporation is oxygen-pressure dependant ($P(O_2)^{3/4}$) [16] and thinning of the scale affects its the protective aspect. Authors generally insist more on the influence of temperature than of partial pressure of oxygen on oxidation, as the differences seem to be more obvious. Kumar et al. [17] who worked on IN625 (an alloy of composition close to IN617) in the temperature range 600–1250 °C affirm that no change in oxidation mechanism is expected between oxidation at 1 bar of O_2 and 1.2 mbar of O_2. To explain that, they argue that the equilibrium oxygen partial pressure for each oxidation reaction is orders of magnitude smaller than the $p(O_2)$ used in their work (4.7×10^{-8} mbar for Ni, the highest equilibrium $p(O_2)$ among all the oxides).

In this case, the supply of oxygen is not a limiting step, which means that the reactions are controlled by solid-state diffusion processes [18]. However, in some cases, the rate-determining factor is the adsorption of oxygen on the metal surface. This can be the case at very low oxygen partial pressure, where the rate of reaction is directly proportional to collision of oxygen molecules, or "impingement rate". At higher partial pressure, the oxidation rate can be limited by the dissociation step of the O_2 molecules into adsorbed atoms, prior to the reaction.

This could explain the preferential or selective oxidation that takes sometimes place at reduced partial pressure of oxygen [18], that is, under conditions where the availability of oxygen at the surface is limited. In general, the lower the ambient oxygen activity, the lower are the less noble elements concentrations needed to achieve selective oxidation. A low partial pressure of oxygen will for example allow chromium to be highly selectively oxidized in a Ni–Cr alloy [19] even though NiO is stable under the oxidizing conditions.

Therefore, to understand the influence of partial pressure on the composition of the scale and on the oxidation mechanisms, tests were carried on IN617 at 850 °C using three different partial pressure of O_2 of completely different ranges: 10^{-5} mbar (low partial pressure), 0.2 mbar (medium partial pressure) and 200 mbar (high partial pressure). Duration of the different tests, from 1 to 336 h, was chosen in order to understand the growth mechanism with an increasing time of oxidation. The obtained oxide layers were then characterized using different techniques of surface analysis such as XRD, XPS, GD-OES, SEM, EDX in order to know the oxide scale morphology for the different partial pressure used and to understand the oxide growth mechanisms.

Experimental

Material

Composition of the Inconel 617 alloy is shown in Table 1.

Table 1 Composition of alloy Inconel 617 used for the experiments (from the supplier certificate)

Elm.	Ni	Cr	Co	Mo	Al	Fe	Ti	C	Si	Mn	B	P	S
at.%	Bal.	24.13	11.85	5.58	2.21	0.98	0.51	0.28	0.27	0.11	0.011	<0.009	<0.002

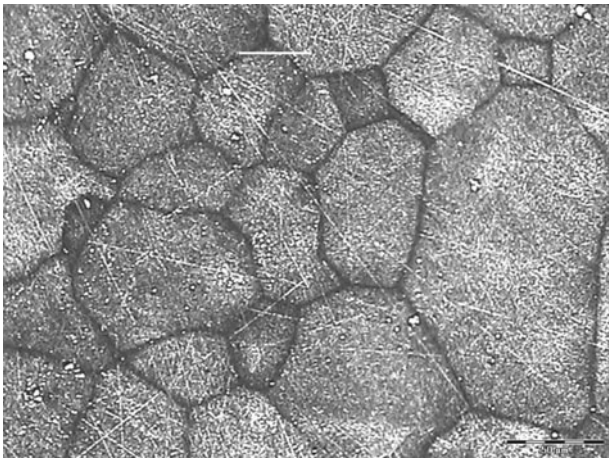

Fig. 1 Optical microscope observation after etching of the as-received microstructure of IN617 (magnification ×200)

The as-received microstructure was observed with an optical microscope after chemical etching with Kalling's reagent (Fig. 1). The area of the grains was statistically measure with the analySIS software from Soft Imaging System and an average of 70 μm was found for the grain size.

Sample size is a thickness of 2 mm and a square shape of 10 × 10 mm. Each coupon is polished down to 1 μm alumina powder and ultrasonically degreased in an ethanol–acetone mixture. Oxidation is then carried out in three different oxygen atmospheres.

Samples oxidized at a low O_2 partial pressure are previously annealed for 3 h at 1000 °C in vacuum in order to obtain a clean metallic surface. It was found that annealing affects the microstructure: the grain size is increased to 90 μm and EDX analysis shows that precipitation of carbides occurs at the grain boundaries. The microstructure and secondary phases of IN617 after heat treatments has been studied previously [20, 21] and these carbides were identified as $M_{23}C_6$ type with M being chromium and molybdenum. However, a comparison of the first oxidation stages shows that after 30 min of oxidation at 1×10^{-5} mbar behaviour of the annealed and non-annealed samples, the composition of the oxide layer formed is similar.

Experimental Set-Up

Three different partial pressure of O_2 are used in this study. A "low" $p(O_2) = 1 \times 10^{-5}$ mbar, a "medium" $p(O_2) = 0.2$ mbar and a "high" $p(O_2) = 200$ mbar (air). The temperature of oxidation applied is 850 °C for each case.

In the case of the low $p(O_2)$, oxidation takes place in a UHV chamber of a X-ray Photoelectron Spectroscopy apparatus which comprises a preparation chamber equipped with an electron bombardment heating system. The gas is introduced with a leak valve and the chamber pressure is raised until 10^{-5} mbar.

Oxidations at a medium $p(O_2)$ occur in a tube furnace with a flowing Ar-O_2 gas mixture containing 100 ppm of O_2 from Messer. The O_2 content is regularly measured with gas mass spectrometry and is between 0.1 and 0.2 mbar.

A muffle furnace is used for oxidation in air (200 mbar).

Characterization Techniques

X-Ray Photoelectron Spectroscopy

Analysis were carried out using a Thermo MKII and a Thermo Escalab 220i XL spectrometers, both with an un-monochromatic Al Kα radiation with an incident energy of 1486.6 eV. The pass energy used was 100 eV for the overview spectra and 20 eV for the detail areas of the different elements. The charge effect was corrected using C 1s peak fixed at 285.0 eV due to the atmospheric contamination.

X-Ray Diffraction

XRD analysis were performed on a X'Pert MPD from Panalytical with a cobalt anticathode emitting two wavelengths: K-α1 = 1.78897 Å and K-α2 = 1.79285 Å. $\theta/2\theta$ and glancing angle (1° up) analysis were conducted and then data was processed with a X'Pert highscore v 2.2.0 software from Panalytical. The database used to retrieve the phases is PDF-2 Release 2005.

Scanning Electron Microscopy

SEM observations were made on a JEOL JSM 7000F. Imaging was done on the secondary electron image mode with an acceleration tension of either 10 or 15 kV. The EDX system used was Spirit from Princeton Gamma Technology. EDX analyses were carried out at 10 or 15 kV and quantification could be obtained thanks from the Spirit software standards library.

Glow Discharge Optical Emission Spectroscopy

GD-OES analyses were performed with two different instruments. The first one was a JY 50S from Jobin–Yvon with a radio-frequency generator Sairem. The second one was a GD Profiler 2 by Horiba Jobin–Yvon. The software used was Quantum XP. High purity argon was employed as a discharge gas. The first series of analysis was done with a radio-frequency power of 50 W and the second with a radio-frequency power of 30 W.

A calibrated method was especially created with all elements of interest, including oxygen.

On of the main difficulty in the quantitative study of oxide layers with GD-OES is the lack of certified standards containing known amount of oxygen. In this work, calibration of oxygen was obtained using well-characterised oxide-coated samples. With density and sputtering rate of the calibration samples, the software Quantum XP is able to convert the erosion time into a erosion depth. However, porosity, together with continuous change of composition can induce some imprecision in converting the sputter time into depth value. Therefore, samples were eroded until the oxide-matrix interface, and craters depth were measured systematically. The "Crater measurement" option on the quantum XP software was then used in order to improve the accuracy.

Results

Low Partial Pressure: 10^{-5} mbar

Tests have been carried out at 4 different oxidation times: 1, 24, 96 and 140 h.

SEM Imaging

Observation of the oxide surface of the different samples shows nodule-shape structures that grow with increasing oxidation time, covering the entire surface (Fig. 2). EDX mapping showed that the oxide layer is continuous: the metal surface is covered with oxide and there is no difference in composition between the nodule-shape structures and the underlying oxide. As their size increase with higher time of oxidation, this shows that the nodule-shape oxide growth occurs by cationic diffusion from the matrix to the oxide-gas interface. The high concentration of excrescences at the grain boundaries is an evidence of an enhanced outward diffusion of cation at the grain boundaries.

Cross-section observation of the sample oxidized for 96 h shows that the thickness of the scale is about 0.5 μm (Fig. 3).

XRD Analysis

Two groups of peaks were detected on diffractometers of the samples oxidized at low partial pressure of O_2 (Fig. 4). A previous analysis of the as-received alloy allowed us to identify the group of peaks corresponding to the metallic matrix. The relative intensity of the matrix peaks decreased with an increasing oxidation time, as a result of a thickening of the oxide. The other phase was identified as chromium oxide Cr_2O_3 (Fig. 4).

XPS Analyses

The XPS technique allows us to determine the composition of the extreme surface of the oxide (depth of analysis <10 nm). Determination of the speciation of the detected chemical elements is also possible.

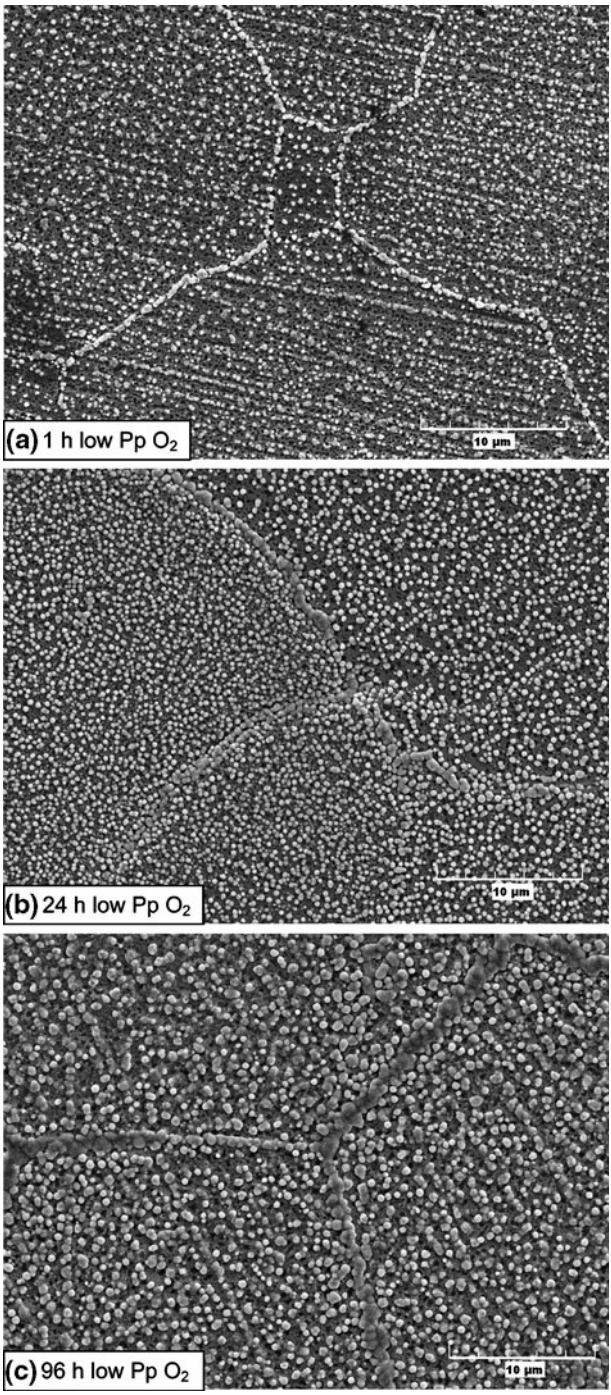

Fig. 2 SEM image (magnification ×3,000) of the surface of the oxide formed at 10^{-5} mbar of O_2 for **a** 1 h, **b** 24 h and **c** 96 h

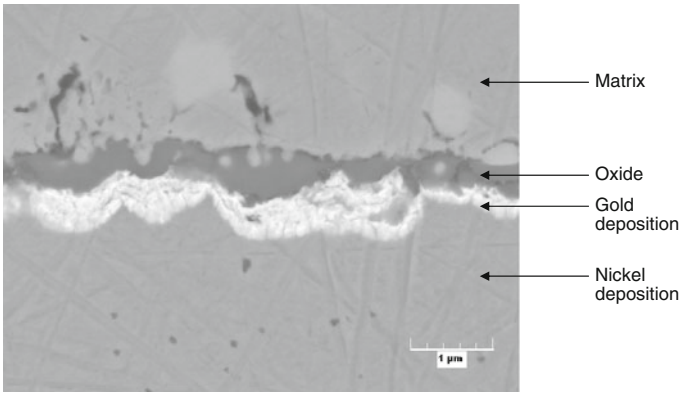

Fig. 3 SEM image (magnification ×20,000) of the cross-section of the 96 h test sample at 10^{-5} mbar of O_2

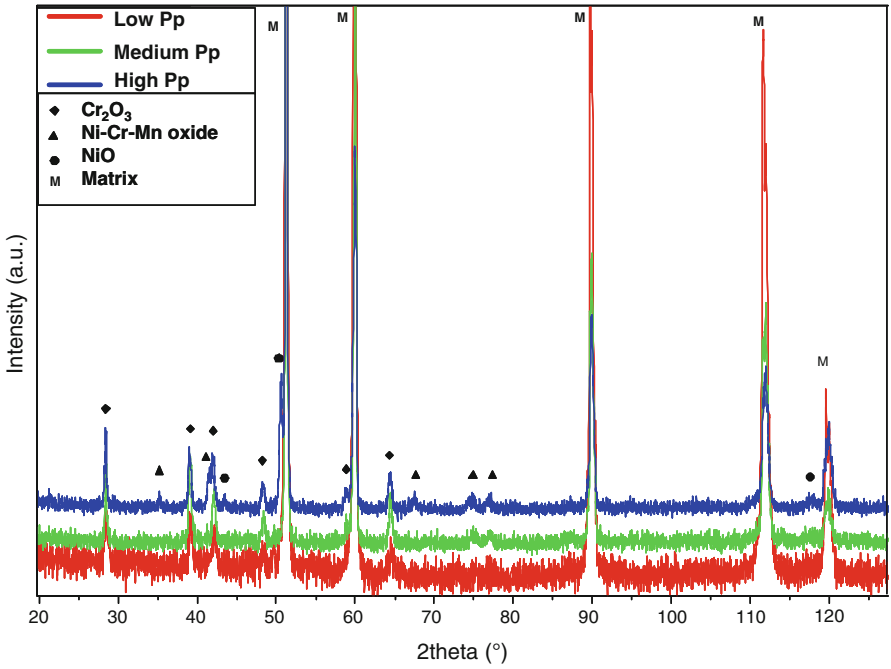

Fig. 4 XRD diffractometers of samples oxidized for 96 h in the 3 different O_2 atmospheres: 10^{-5} mbar, 0.2 mbar and 0.2 bar

No elements in the metallic form were detected at the surface from 1 h of oxidation. That means that the oxide layer is continuous and its thickness is more that 10 nm.

Oxides were identified by deconvolution of individual spectra of the elements. The Cr-$2p_{3/2}$ spectra can be fitted with three peaks of energy 576.3 ± 0.3,

Table 2 Evolution of the extreme surface composition with time for the low O_2 partial pressure tests (from XPS analysis, using Scofield sensibility factors)

Elements (at.%)	1 h	24 h	96 h	140 h
Cr	78	91	97	100
Ti	9	9	3	0
Al	13	0	0	0

577.5 ± 0.3 and 579.1 ± 0.3 eV corresponding to chromine Cr_2O_3. Biesinger et al. [22] found a deconvolution consisting of a five multiplet peaks under high spectral resolution condition. But considering the present apparatus resolution, a deconvolution with three peaks is suitable. Al_2O_3 was identified with a peak at 119.5 eV ± 0.3 eV on the Al-2s core level spectra [23]. Deconvolution of Ti-2p core level spectra consisted of a doublet of energy 458.8 ± 0.3 eV ($2p_{3/2}$) and 464.1 ± 0.3 eV ($2p_{1/2}$). These binding energies are characteristic of TiO_2 oxide [24–26].

The evolution of the extreme surface composition with time can therefore be obtained (Table 2: quantification does not include O). From the first hour of oxidation, the major oxide is chromium. Titanium and aluminium oxide contents decrease with time in favour of chromium. Thus, the external part of the oxide is composed of a large majority of chromium oxide containing titanium oxide firstly, and finally composed of only chromium oxide as the layer thickens. The internal part, at the matrix-oxide interface is enriched with aluminium oxide.

To confirm that, some very short time test were done in the same conditions with an in situ XPS analysis. Al_2O_3 appears to be the main oxide until 4 min of oxidation for a non-heat-treated sample. The evolution of the composition calculated from in situ XPS analysis is presented in Fig. 5 for the 10 first minutes of oxidation.

Medium Partial Pressure

Tests under medium partial pressure of oxygen were held at different times: 96 h, 10 days and 28 days.

SEM Imaging

The nodule-shape structures existing at low partial pressure oxidation are observed at medium partial pressure too. In the same manner, an enhanced growth in the grain boundaries area is observed for the two shortest tests, but not for longer oxidation time as the nodules grow and end up joining together, covering the entire surface (Fig. 6).

GD-OES Analysis

Samples oxidized at medium partial pressure were analysed with GD-OES. The different profiles obtained for different oxidation times show the same features, with

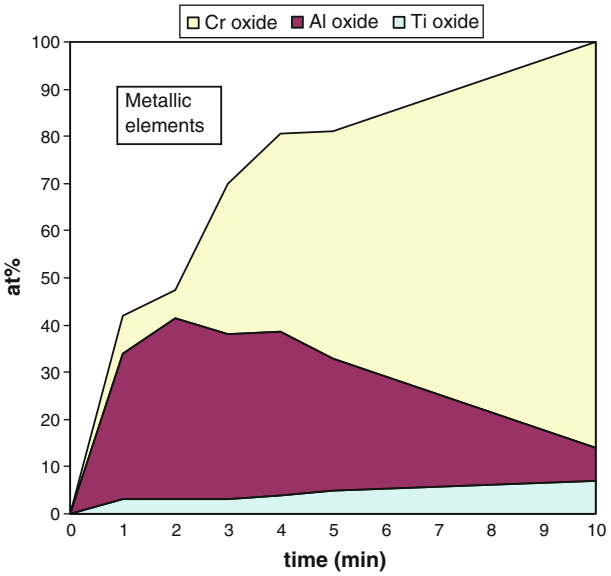

Fig. 5 Evolution of the oxide surface composition during the first minutes of oxidation at 10^{-5} mbar of O_2 (measured by XPS analysis)

a thickening of the chromium oxide layer with time. Figure 7, corresponding to the sample oxidized for 28 days shows the main characteristics of the oxide layer obtained at medium partial pressure.

The oxide layer mainly contains chromine. Titanium is enriched in the chromine layer, and particularly near the surface. Manganese segregates as well at the surface and reaches a rather high content but, unlike titanium, is not present all through the oxide layer. There is a clear enrichment of aluminium at the matrix-oxide interface. On the sample oxidized for 28 days, one can notice that the content of nickel, and in a smaller extent the content of cobalt increase near the oxide surface. This is not observed for the shorter tests in these conditions.

XPS Analysis

Analysis of the extreme surface shows that the oxide layer is continuous from 96 h of oxidation as no metallic element is detected.

Various elements are found in the oxide surface. Ni-2p spectrum deconvolution allows identifying NiO with a $2p_{3/2}$ peak at 854 ± 0.3 eV and two satellites peaks at 856.3 ± 0.3 and 861.8 ± 0.3 eV. There is a third shake-up satellite peak, but in the present case it was too small to be distinguished [27]. The Co-2p spectrum corresponds to CoO oxide with a $2p_{3/2}$ peak binding energy of 780.8 ± 0.3 eV and a satellite peak at 786 ± 0.3 eV [28]. MoO_3 is found with doublet peaks energy of 232.6 ± 0.3 eV ($3d_{5/2}$) and 235.7 ± 0.3 eV ($3d_{3/2}$) [28, 29]. MnO_2 is identified with a $2p_{1/2}$ peak of energy 652.6 ± 0.3 eV [28].

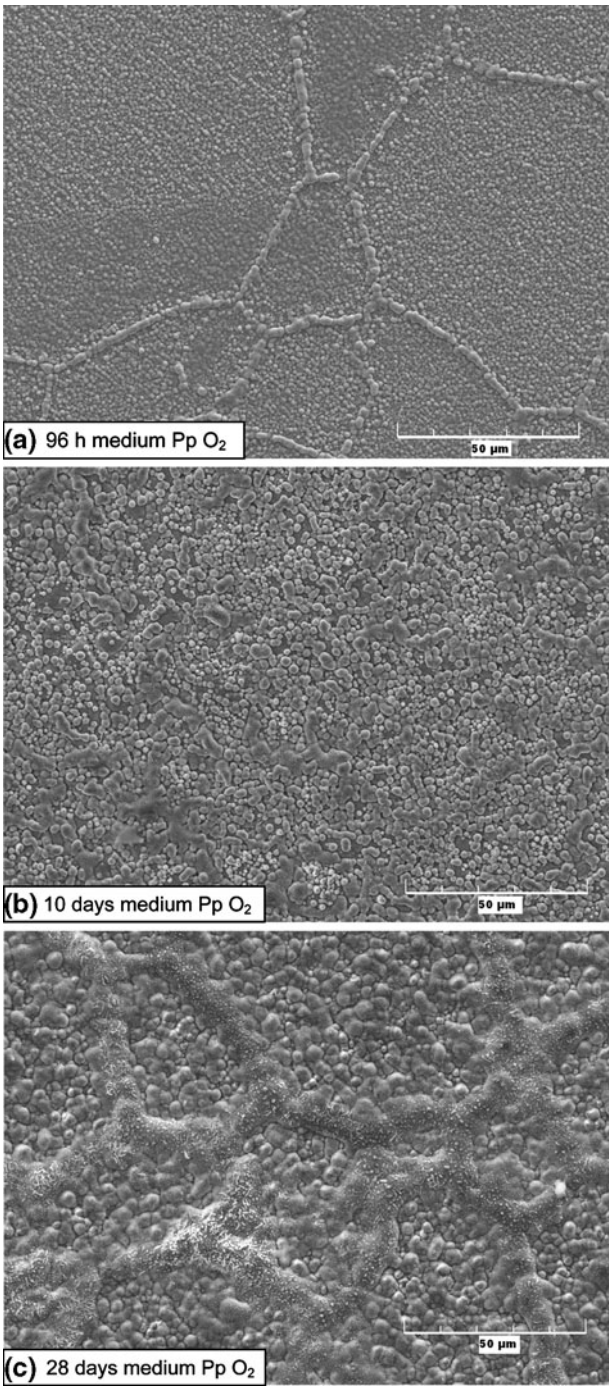

Fig. 6 SEM image (magnification ×1,500) of the oxide surface of the **a** 96 h test sample, **b** 10 days test sample and **c** 28 days test sample at medium O_2 partial pressure

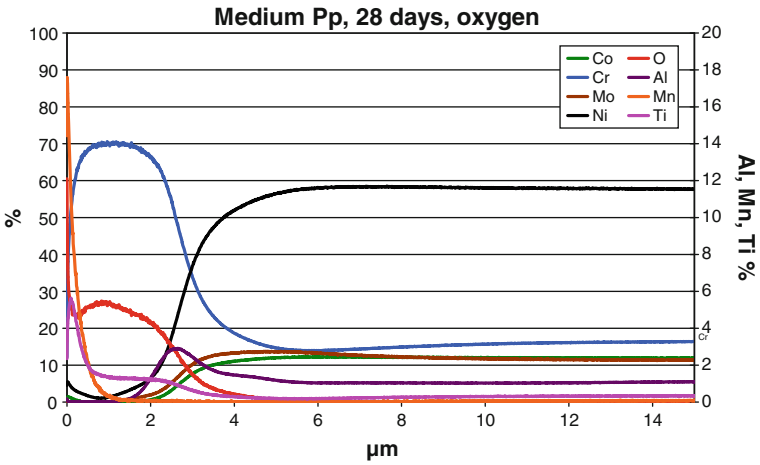

Fig. 7 GD-OES calibrated depth concentration profile of the 28 days test sample at medium O_2 partial pressure (wt%)

Table 3 Evolution of the surface composition with time obtained by quantification of XPS analysis for the samples tested at 0.1 mbar of O_2

Elements (at.%)	96 h	10 days	28 days
Ni	3	3	11
Cr	63	59	49
Co	–	1	3
Mo	3	5	3
Al	8	–	–
Ti	19	25	24
Mn	4	7	10

Detail areas spectrum for Cr, Ti and Al shows similar peaks as the one for low partial pressure oxidation. Cr, Ti and Al oxides are exactly the same as found in the low O_2 partial pressure: Cr_2O_3, TiO_2 and Al_2O_3.

The evolution of the composition is shown in Table 3 and confirms the previous observations on the scale morphology obtained from the concentration profiles. Chromium is the major element then the major oxide is Cr_2O_3. The level of titanium increases with oxidation time, and this shows that titanium oxide segregates at the surface. Aluminium is detected for the shortest times of oxidation, as Al_2O_3 is located near the matrix-oxide interface. Manganese content appears to increase at the surface with longer time of oxidation and reaches 10% for the longer one. That demonstrates that MnO_2 oxide segregates at the surface. Ni content increases slightly for the longest test: NiO extreme surface content eventually increases with time of oxidation.

EDX Analysis

EDX results of the surface of the oxide are presented in the Table 4. As the depth of analysis is quite important compared to the thickness of the oxide layer (around

Table 4 Evolution of the surface composition with time obtained by EDX analysis for the samples tested at 0.1 mbar of O_2

Elements (at.%)	96 h	10 days	28 days
Ni	13	5	3
Cr	72	85	85
Co	3	1	1
Mo	2	1	–
Al	4	1	–
Ti	2	3	4
Mn	1	3	6

0.6 μm for the 96 h test), the contribution of Ni, Co and Mo for the shortest tests could be a contribution from the matrix, and this in spite of the presence of these elements in the oxide. Chromium is the major element. A small amount of nickel is contained in the oxide. Mn appears for the longest oxidation time. The content of Ti increases slightly with oxidation time, but is kept quite low compare to its very high content measured from XPS quantification. This demonstrates that Ti is located on the extreme surface of the oxide. Aluminium is detected for the shortest tests, and this is coherent with the fact that aluminium oxidation takes place at the matrix-metal interface.

XRD Analysis

The previously identified chromia and matrix phases are detected on the diffractograms.

Another phase is found, which seem to be a mixed oxide of Ni, Cr and Mn (Fig. 4). Due to the complexity of the alloy and the various possible combinations of oxidized elements, many candidate phases are fitting this group of peak, this one being the most coherent with the observed enrichment of Mn and Ni at the surface observed in XPS.

High Partial Pressure

Four different time of oxidation were used for the high partial pressure tests: 24 h, 48 h, 96 h, and 14 days.

SEM Imaging

The observation of the oxide surface with SEM reveals a surface state completely different from the previous oxidation atmospheres. The dominant aspect was fine sharp grains (Fig. 8). The matrix grain boundaries are most of the time clearly noticeable. The oxide layer of the sample oxidized for 24 h presents many cracks. In general, the oxide surfaces for all times of oxidation are really irregular.

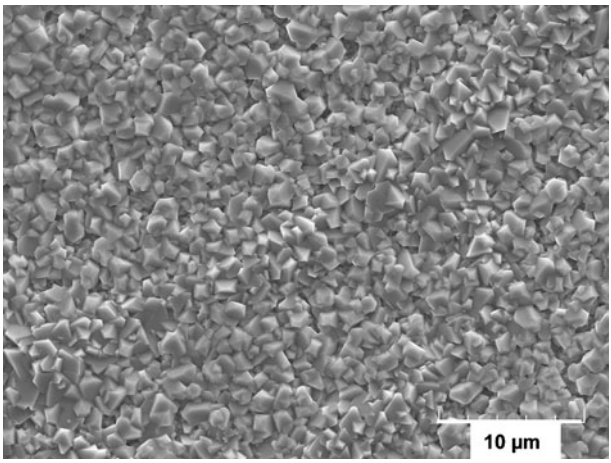

Fig. 8 SEM image (magnification ×3,000) of the 48 h test sample at high O_2 partial pressure

XPS Analysis

The composition of the extreme surface of the oxide does not change with the time of oxidation, either for the oxides nature, either for their quantification.

Concerning the nature of the species, the same oxides as for the medium partial pressure tests are found: NiO, Cr_2O_3, CoO, MoO_3 and TiO_2. The quantification of the element (excluding O) shows a constant composition for the different tests. The sample oxidized 48 h at high oxygen partial pressure surface composition is Ni (57%), Co (21%), Cr (13%), Mo (5%) and Ti (4%).

XRD Analysis

The same phases, corresponding to chromia, the matrix, and a Ni–Cr–Mn oxide are found on the high partial pressure tests. However, a new phase appears on the diffractometers, identified as nickel oxide NiO (Fig. 4). The intensity of the group of peaks corresponding to this phase decreases with time of oxidation, while the one corresponding to the chromia phase increases.

EDX Analysis

There are no clear differences or evolution with time in the results of EDX analysis of the oxides surfaces of the different samples. Table 5 shows the surface composition of 2 samples oxidized for 24 h and 14 days. The high quantity of chromium detected shows that the NiO layer at the extreme surface is thin (<1 µm, the EDX depth of analysis) and that there is a chromine layer underneath. A small raise of the manganese content is observed with time.

Table 5 Surface composition obtained by EDX analysis for two different time of oxidation at 0.2 bar of O_2

Elements (at.%)	24 h	14 days
Ni	51.7	44.0
Cr	30.0	32.1
Co	12.6	15.4
Mo	0.5	0.1
Ti	0.8	0.9
Al	2.1	2.2
Fe	1.2	2.1
Mn	1.1	3.3

GD-OES Analysis

In order to understand the evolution of the layer with time, quantified concentration profiles of the different elements for 3 tests are presented: 24 h test, 48 h test and 14 days test (Fig. 9).

One can see on Fig. 9a that the oxide layer of the sample oxidized for 24 h is composed of a mix of nickel and chromium oxide. Near the surface, the nickel is predominant, and underneath, both of them are in the same quantity. There is a slight enrichment of cobalt and manganese at the surface, and of aluminium at the oxide-matrix interface.

On Fig. 9b, there is a clear stratification of the oxide layer. The external part is a majority of nickel enriched with cobalt and manganese. A mixed oxide lies underneath this external part and compose the thicker part of the layer. This mixed oxide is composed of chromium for a great majority, as well as nickel. The whole layer benefits of a slight enrichment of titanium and, as for the sample oxidized during 24 h, aluminium oxidize at the interface oxide-matrix.

The GD-OES analysis of the sample oxidized for 14 days, corresponding to Fig. 9c, presents the same characteristics as the previous tests: The external part of the layer is composed of a majority of nickel oxide, enriched with cobalt and manganese. Under this external layer, lies a thicker layer of an oxide composed of mainly chromium oxide, with an enrichment of aluminium at the matrix interface. Some changes can therefore be observed: the chromium layer no longer contains nickel, and titanium segregates at the surface. Moreover, it should be noted that a thickening of the oxide is observed, but that this thickening only concerns the sub-part of the oxide, i.e. the chromium-rich sub-layer of the oxide. This explains the decrease of intensity of the peaks of the NiO phase on the XRD analysis: the thickening of the chromia layer underneath the Ni-rich external layer results in a decrease of NiO concentration, thus in the phase intensity.

Discussion

Growth Mechanisms of the Oxide Layer

Several models of simple alloys, such as Ni–Cr, Ni–Al binary alloys or Ni–Cr–Al ternary alloy have been extensively studied in order to predict the oxide layer that

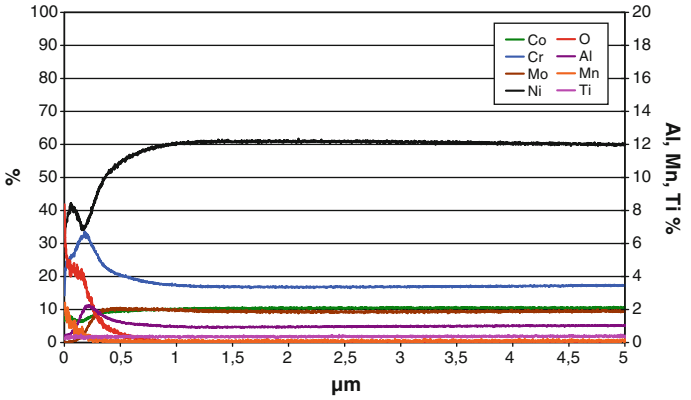

(a) High Pp, 24 hr, oxygen

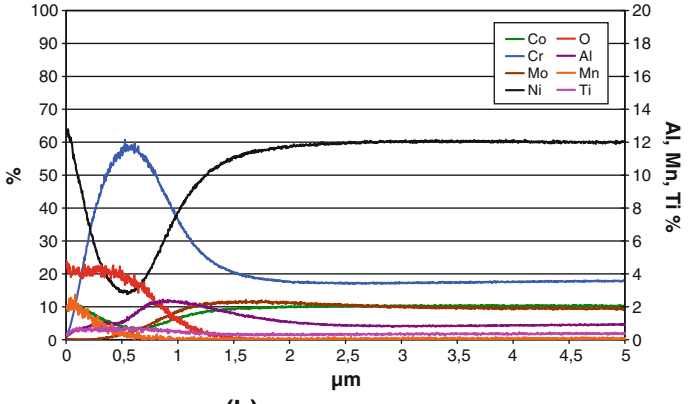

(b) High Pp, 48 hr, oxygen

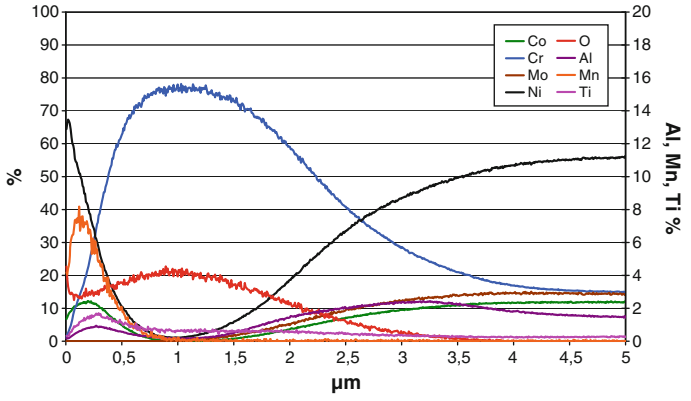

(c) High Pp, 14 days, oxygen

Fig. 9 GD-OES calibrated depth concentration profile for sample oxidized at high O_2 partial pressure (wt%) for **a** 24 h, **b** 48 h and **c** 14 days

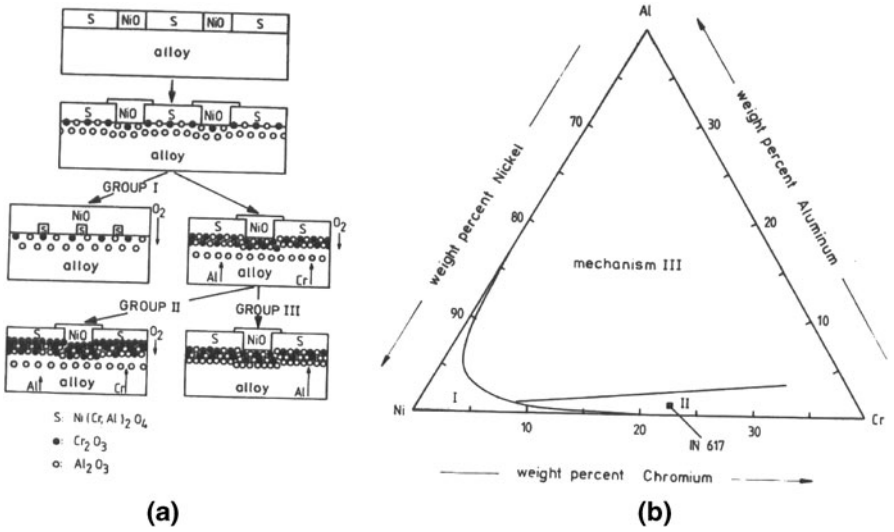

Fig. 10 The oxidation of Ni–Cr–Al after Giggins and Pettit [30]. **a** The 3 mechanisms depending on the alloy group. **b** Oxide map at 1000 °C showing the oxidation mechanism followed as a function of the alloy composition

will form depending on the alloy composition. According to Christ et al. [15], additional components Mo and Co do not affect IN617 oxidation, thus the present alloy can be seen as a Ni–Cr–Al type alloy. Giggins and Petit [30] have studied oxidation of Ni–Cr–Al alloys between 1000 and 1200 °C and were able to distinguish 3 different mechanisms that are summarized in oxide maps. Those maps are not thermodynamic diagrams but are based upon kinetic processes that take place during the scale development. If one neglects the Co and Mo content in IN617, the alloy can be classified from its Cr and Al content as a group II alloy (see Fig. 10b). The mechanisms proposed by Giggins and Pettit [30] are presented on Fig. 10a. For group I alloys, the content of Cr and Al is too small to form and dense film, so these elements will suffer internal oxidation. NiO will form the layer. For group III and group II alloy, a rapid uptake of oxygen at the beginning of oxidation will convert the surface of the alloy into oxide that mainly contains Ni (the base element). Cr_2O_3 and Al_2O_3 precipitate beneath the external scale. For group III alloys, the volume of Al_2O_3 precipitate is sufficient to form a continuous layer. For group II alloys, the content of Al is too low, so Al_2O_3 will oxidize internally while Cr will diffuse above the duplex scale. The steady state conditions are reached when Cr diffuses through the chromia scale to grow externally.

This latter mechanism is expected for IN617 (Fig. 10b). However, some precautions have to be taken. Firstly the model was established at 1000 °C while the present study was carried out at 850 °C. Secondly, neglecting Mo and Co content changes the whole composition by artificially increasing the content of Ni on the ternary diagram. Moreover, Co is found in the transient oxide film [15] and therefore its role can not be totally neglected. Finally, the oxide maps were established at 0.1 atm of oxygen. In the present work, some differences between the

3 different ranges of O_2 partial pressure were observed. These differences concerning the growth mechanisms and the scale composition are discussed and detailed below.

Internal Aluminium Oxidation

Results from the XPS analysis of low partial pressure oxidation and concentrations profiles obtained from GD-OES of the different tests demonstrate that aluminium oxides are located in the matrix-oxide interface area. This is in agreement with previous work on alloy 617 [13, 14] and with the prediction model of Ni–Cr–Al [30] where it was found that Al forms internal oxide at the grain boundaries. There are three necessary conditions to form internal oxides of an alloying element [31]. The first one is a lower energy of formation of the internal oxide than the external oxide. One can see in the Elligham–Richardson diagram (Fig. 11) that Al oxide energy of formation is lower than the one of Cr oxide. The second one is a large negative

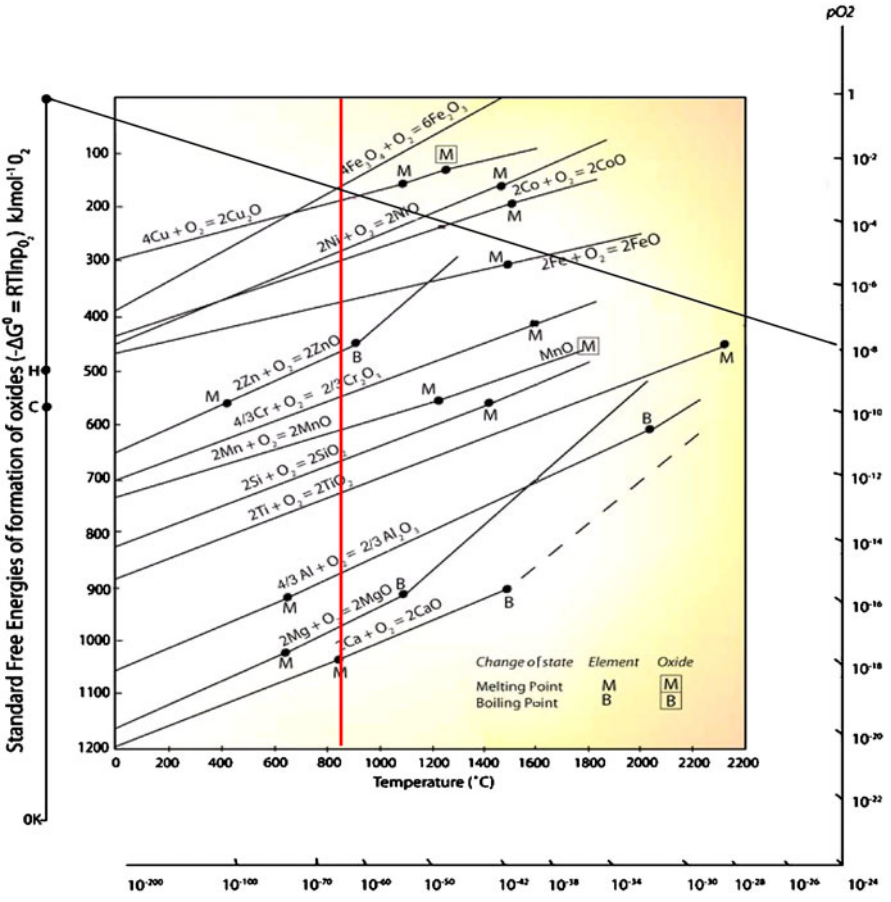

Fig. 11 Ellingham–Richardson diagram [43]

value of this energy of formation. The Ellingham–Richardson diagram shows that Al oxide has the lowest Gibbs energy of formation among all the alloying elements of the alloy. The third condition is a low concentration of the element in the alloy compared with the other oxidizing elements. IN617 contains 1.1 wt%, which is a low content compared to the contents of Ni and Cr and which is, according to Smialek and Meier [32], not sufficient to form an external and continuous oxide layer.

Cationic Growth of the Oxide Layer

Several evidences are pointing out to the conclusion that in the case of low and medium partial pressures the oxide grows by outward cationic diffusion of metallic species. The SEM observation shows that nodule-shape structures develop over a continuous oxide that lies on the metal surface and through which the cations Cr^{3+} must therefore have diffused. Moreover, the XPS analysis of the oxide surface reveals that aluminium oxide is detected only for short times of oxidation, and that the chromium oxide content increases with time. And yet, the oxide layer structure is enriched with aluminium oxide at the matrix-oxide interface and the outer part mainly contains chromia. This shows that the new growing oxide covers the existing oxide with time, in accordance with an outward growth mechanism. Finally, a complementary experiment has been carried out. A silver layer was plated on an IN617 sample and the sample was exposed to an oxygen medium partial pressure. In-depth concentration profiles of the various elements were then obtained using GD-OES analysis. The concentration profile versus sputtering time graph (Fig. 12) clearly shows that the silver is located at the matrix-oxide interface after oxidation. This proves that the growth takes place by outward diffusion of metallic cations, through the Ag deposit, toward the surface.

This is in accordance with Wood [33] model of oxidation of a binary alloy A–B, with B being the less noble metal. If IN617 if simplified into a A–B binary alloy, A representing Ni and B, Cr. When oxidizing IN617 at 850 °C, the obtained scales at low and medium partial pressure contain mainly, if not exclusively for the low Pp chromium oxide. Wood says that when the general conditions permit B to be the only element oxidized, even if AO can oxidize in the prevailing conditions, the layer of BO grows exclusively externally. However, in practice, small amount of AO are present in the scale, producing doping effects.

Low O_2 Partial Pressure Tests: Selective Oxidation

When exposed to medium and high partial pressure of oxygen, oxides of various elements are formed. In the case of tests performed at low partial pressure of oxygen, only three elements are found in the oxide: Al, Ti and Cr. This result is in good agreement with the work of Jo et al. on the same alloy at a O_2 partial pressure of 4.7×10^{-4} mbar. They exposed IN617 at 1050 °C for 2000 h. They found an oxide layer composed of mainly chromine that contained small amount of TiO_2 and internal Al_2O_3 [13]. However, comparison with our results is not really possible, as at 1050 °C evaporation of the chromium oxide CrO_3 occurs.

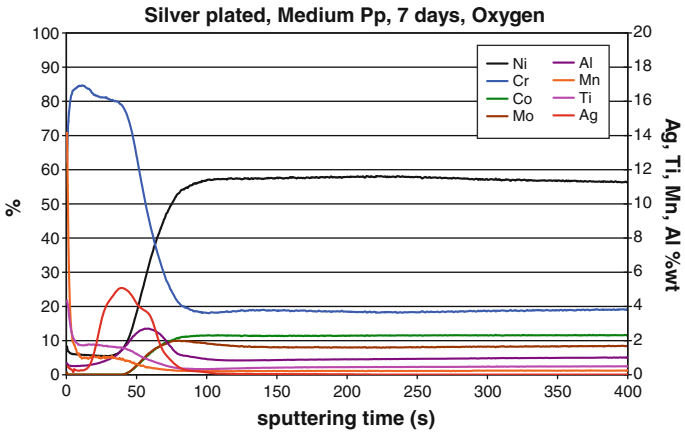

Fig. 12 GD-OES calibrated concentration profile (O quantification not included) with sputtering time of a sample oxidized 7 days at 0.1 mbar of O_2—sliver plated

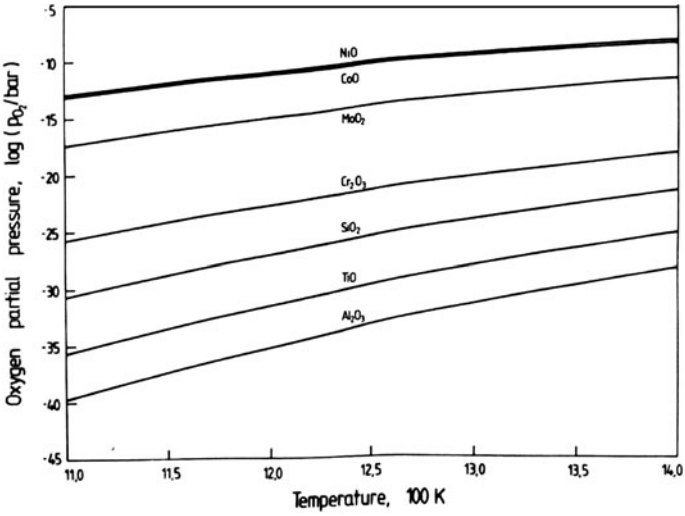

Fig. 13 Equilibrium oxygen pressure for the formation of various oxide of elements in IN617 depending on temperature [15] (data calculated from [34])

Figure 13 [15] shows the dependence of the equilibrium oxygen pressure on temperature for oxide formation. Calculation were made from thermodynamic data [34] for the alloying elements of IN617 with the approximation that the initial activity of the element equals the mole fraction. It is clear that at 850 °C and 10^{-8} bar of O_2, oxides of all the alloying elements are stable. In the present case, a selective oxidation takes place: in other words, reactions with the lower standard free energies of formation occur. These more stable oxides appear to be Al, Ti and Cr oxide.

However, it is important here to consider the fact that the experiments at low partial pressure of O_2 were carried out under vacuum. The "pressure gap", difference of decades between the UHV experiments and the industrial application has already questioned the scientific community, particularly in the heterogeneous catalysis field where the total pressure of the system has been found to have an influence on the reaction products [35, 36]. An explanation for these differences can be found with surface chemistry. When a molecule reaches the metallic surface, the key factor for its absorption on this surface is a sufficient translational energy. Firstly, the rate of the reaction being limited by the flux of incident molecules with sufficient energy, high pressure increases the absolute number of high energy molecules, thereby increases the reaction rate. Moreover, the inert gas atoms play a role on the dissociation by pounding the already adsorbed molecules, inducing the dissociation of the adsorbent (collision-induced absorption, collision-induced desorption) [37, 38]. The present tests were carried out under vacuum and without an inert gas. The experimental conditions may decrease the surface reaction rate and explain the observed selective oxidation.

Rate of Diffusion Versus Thermodynamical Stability

Under a medium oxygen partial pressure atmosphere, various oxides form on the alloy surface, as seen with XPS results. All are thermodynamically stable and at this medium partial pressure of O_2, the selective oxidation of the more active elements that took place under the low O_2 partial pressure tests does not occur. TiO_2 is localized at the extreme surface, but when increasing the time of oxidation, the oxide layer that thickens with time is composed of mainly chromium, as predicted by the Ni–Cr–Al model of Giggins and Pettit [30]. Indeed, among the most active elements, chromium is the element which has the highest content in the alloy. Therefore the supply of chromium cations to the oxide layer is very important compared to minor elements. However, for the longer oxidation time (28 days) nickel and manganese are found to be enriched in the outer part of the scale. This can be explain by the diffusion rates of these two elements in Cr_2O_3: Lobnig et al. [39] showed that at 900 °C manganese has a lattice-diffusion coefficient in a chromia layer grown on a Fe–20Cr–12Ni about two orders of magnitude higher than chromium ($D = 1 \times 10^{-14}$ cm^2 s^{-1} for Mn and $D = 8 \times 10^{-16}$ cm^2 s^{-1} for Cr autodiffusion for a 4 h annealing time), and work from Sabioni et al. [40] showed that diffusion rate of nickel is higher than autodiffusion of chromium in chromine at 900 °C.

It was established previously that growth of the scale at this range of partial pressure occurs by outward diffusion of metallic cations. Elements with the faster diffusion, such as nickel and manganese diffuse through the scale to form a layer on top of the chromium scale. The same explanation is probably available to explain the presence of cobalt on the surface.

This phenomenon is likely to be enhanced, if not caused by the chromium depletion that occurs in the sub-scale area. This well known phenomenon, which can be observed on the concentration profiles of the elements obtained by GD-OES analysis of the sample oxidized for 28 days at medium O2 partial pressure, takes

place when the chromium oxide is outwardly growing. The near-surface chromium diffuses toward the oxide, resulting in a depletion of this element in the sub-scale area. It is probable that this depletion has favoured the external diffusion of other elements such as Ni and Mn.

Case of the High Oxygen Partial Pressure

According to Jang et al. [12], oxides formed in air are less dense than oxides formed in impure He, i.e. at lower O_2 partial pressure. When growing an oxide layer for 100 h at 900 °C, they observed a same weight gain, but a thicker oxide for the sample exposed to air than for the one exposed to impure He. Adding to this the fact that air-oxidized samples showed a larger penetration depth of internal oxides, it is clear that the oxide layer is therefore less protective to further oxidation. If breaking of the oxide layer occurs and it is no longer continuous, elements from the matrix can then be exposed and oxidized. However, this argument can not be applied to our condition. Ni predominates at the scale surface from the 24 h oxidation test at high partial pressure of O_2. As Ni is detected in the scale from the early stages of oxidation, its presence can not indeed arise from a breakaway or a discontinuous oxide layer.

The phenomenon of transient oxidation looked into by Wood and Chattopa [41, 42] seem to be a more suitable mechanism. The initial oxide formed on an alloy is produced by impingement of molecules from the oxidizing gas, creating nuclei of simple or complex oxides produced approximately in the ratio of the composition at the alloy surface, i.e. the alloy composition. Considering that all the elements of the alloy potentially oxidize, the important factors for an element to land up or not in the oxide layer will be then (1) the content of the element in the alloy (2) the growth rate of the oxides.

The authors looked into the case binary alloys and they considered the growth rate of individual oxides. Ni and Co oxide growth rate is higher than Cr oxide growth rate with typical parabolic rate constants (in $g^2\ cm^{-4}\ s^{-1}$) of 4.1×10^{-11} for Co, 3.9×10^{-14} for Ni (both at 600 °C) and 8×10^{-15} for Cr (at 700 °C). Manganese has a parabolic rate constant higher than these 3 elements: $1.6 \times 10^{-10}\ g^2\ cm^{-4}\ s^{-1}$ at 600 °C [41]. However, as it is a minor element of the alloy its content will be much lower that the other major elements in the scale. Therefore, at relatively high oxygen pressures, a thin outer oxide film of mainly Ni and Co is produced during the first stages of oxidation, which is observed in GD-OES. The authors proposed a mechanism where the outer oxide layer supplies oxygen at its dissociation pressure at the oxide-alloy interface, reducing oxides into metals. The outer scale composition is then constant, as found out with XPS analysis. The next stage then consists in the growth of the thermodynamically favoured oxide Cr_2O_3 that will eventually form a complete healing layer at this interface. This chromia layer thickens with time as shown on the GD-OES concentration profiles. The reduced metal at the surface may be reoxidized and then provide more oxygen to the growing Cr oxide [16]. This transient oxidation is predicted in the Ni–Cr–Al model of oxidation by Giggins and Pettit [30]. However, it is clear that there is a difference between the O_2 medium partial pressure tests,

where the transient step was not observed and the high partial pressure tests, where the transient layer is maintained for the longer tests.

Conclusions

High-temperature oxidation tests were performed at 850 °C in three different range of partial pressure of oxygen in order to investigate its influence on the oxide layer growth mechanisms and composition. In each atmosphere, chromia was the major oxide of the scale. Titanium was found to be enriched in the chromia scale. Intergranular oxides of aluminium were found. The oxide growth was cationic except for the high oxygen partial pressure tests, where the chromia scale thickened under a transient oxide film.

Features for each range of partial pressure were established:

- At 10^{-5} mbar, in spite of thermodynamic stability of every alloy components, a selective oxidation took place. The three more active elements only oxidized to form Al_2O_3 (internally), Cr_2O_3 (major oxide) and TiO_2 (contained in the chromia scale).
- At 0.2 mbar, more species were found in the scale in addition to the 3 previously mentioned oxides: NiO, CoO, MoO_3 and MnO_2. The longest test (28 days) showed that Ni, Mn, and to a lesser extent Co diffused into the scale surface. A long-term oxidation test would be necessary to know if the surface segregation of these species will result in a Ni- and Mn-rich healing layer, or if the thickening of the chromia layer will eventually stop exchanges across the scale.
- Oxidation at 200 mbar of O_2 showed a very different mechanism. The first stage consisted in oxidation of all elements at the alloy surface, forming an outer thin mixed oxide layer that kept a constant composition with increasing oxidation time. This thin layer is believed to provide oxygen to the matrix-oxide interface, where a chromia healing layer will eventually form and thicken with time, following the growth mechanism of transient oxidation.

References

1. W. O. Corwin, et al., *The Gas Fast Reactor (GFR) Survey of Materials Experience and R&D Needs to Assess Viability* (Oak Ridge National Laboratory, 2004).
2. *A Technology Roadmap for Generation IV Nuclear Energy Systems* (U.S. DOE Nuclear Energy Research Advisory Committee and the Generation IV International Forum, 2002).
3. M. Cappelaere, M. Perrot, and J. Sannier, *Nuclear Technology* **66**, 465 (1984).
4. F. N. Mazandarany and G. Y. Lai, *Nuclear Technology* **43**, 349 (1979).
5. W. J. Quadakkers and H. Schuster, *Werkstoffe Und Korrosion-Materials and Corrosion* **36**, 141 (1985).
6. W. J. Quadakkers, *Werkstoffe Und Korrosion-Materials and Corrosion* **36**, 335 (1985).
7. K. G. E. Brenner and L. W. Graham, *Nuclear Technology* **66**, 404 (1984).
8. W. J. Quadakkers and H. Schuster, *Nuclear Technology* **66**, 383 (1984).
9. G. Menken, et al., in *Gas Cooled Reactors Today* (Bristish Nuclear Energy Society, Bristol, 1982).

10. C. Cabet, et al., *Materials and Corrosion-Werkstoffe Und Korrosion* **57**, 147 (2006).
11. H. J. Christ, et al., *Oxidation of Metals* **30**, 27 (1988).
12. C. Jang, D. Lee, and D. Kim, *International Journal of Pressure Vessels and Piping* **85**, 368 (2008).
13. T. S. Jo, et al., *Metals and Materials International* **14**, 739 (2008).
14. D. Kim, C. Jang, and W. Ryu, *Oxidation of Metals* **71**, 271 (2009).
15. H. J. Christ, L. Berchtold, and H. G. Sockel, *Oxidation of Metals* **26**, 45 (1986).
16. I. A. Kvernes and P. Kofstad, *Metallurgical Transactions* **3**, 1511 (1972).
17. L. Kumar, et al., *Oxidation of Metals* **45**, 221 (1996).
18. P. Kofstad, ed., *High Temperature Corrosion* (E.A. Science, 1988).
19. G. R. Wallwork, *Reports on Progress in Physics* **39**, 401 (1976).
20. W. L. Mankins, J. C. Hosier, and T. H. Bassford, *Metallurgical Transactions* **5**, 2579 (1974).
21. S. Rahman, et al., *Materials Letters* **62**, 2263 (2008).
22. M. C. Biesinger, et al., *Surface and Interface Analysis* **36**, 1550 (2004).
23. N. Kosova, et al., *Solid State Ionics* **179**, 1745 (2008).
24. R. M. Wang, et al., *Applied Surface Science* **253**, 8507 (2007).
25. I. Milosev, T. Kosec, and H. H. Strehblow, *Electrochimica Acta* **53**, 3547 (2008).
26. J. J. Blackstock, et al., *Journal of the American Chemical Society* **130**, 4041 (2008).
27. A. P. Grosvenor, et al., *Surface Science* **600**, 1771 (2006).
28. C. D. Wagner, et al., eds., *Handbook of X-Ray Photoelectron Spectroscopy* (Perkin-Elmer Corporation, 1978).
29. F. M. T. Mendes, et al., *Catalysis Today* **133**, 187 (2008).
30. C. S. Giggins and F. S. Pettit, *Journal of the Electrochemical Society* **118**, 1782 (1971).
31. A. S. Khanna, *Introduction to High Temperature Oxidation and Corrosion* (ASM International, 2002).
32. J. L. Smialek and G. H. Meier, in *Superalloy II* (Wiley & Sons, NY, 1987), p. 293.
33. G. C. Wood, *Oxidation of Metals* **2**, 11 (1970).
34. I. Barin and O. Knacke, *Thermochemical Properties of Inorganic Substances* (Springer, Berlin, 1977).
35. M. Baerns, et al., *Journal of Catalysis* **232**, 226 (2005).
36. R. Imbihl, R. J. Behm, and R. Schlogl, *Physical Chemistry Chemical Physics* **9**, 3459 (2007).
37. S. T. Ceyer, *Science* **249**, 133 (1990).
38. J. D. Beckerle, et al., *Journal of Chemical Physics* **86**, 7236 (1987).
39. R. E. Lobnig, et al., *Oxidation of Metals* **37**, 81 (1992).
40. A. C. S. Sabioni, et al., *Philosophical Magazine* **88**, 391 (2008).
41. G. C. Wood and B. Chattopa, *Corrosion Science* **10**, 471 (1970).
42. B. Chattopa and G. C. Wood, *Oxidation of Metals* **2**, 373 (1970).
43. H. J. T. Ellingham, *Journal of the Society of Chemical Industry* **63**, 125 (1944).